J Mater Sci: Mater Med (2007) 18:1185–1193
DOI 10.1007/s10856-007-0138-x

In situ study on the curing process of calcium phosphate bone cement

Yuxing Song · Zude Feng · Ting Wang

Received: 14 October 2005 / Accepted: 23 March 2006 / Published online: 3 February 2007

Abstract The aim of this study was to follow the entire curing process of modified α-TCP cement, and to explore how the liquid phase affects the curing reaction. Two calcium phosphate bone cements (CPCs) with a variety of aqueous solution were studied for comparison. In situ X-ray diffraction analysis and pH testing were employed to follow the chemical reaction, while quantitative ultrasonic measurement (QUS) was carried out to monitor the physical change. Results showed that CPC powders were completely consumed after 72 h. Two steps were presented in apatite formation. The first step was the precipitation of carbonated hydroxyapatite (CHA), and in the second step, conversion of calcium deficient hydroxyapatite (CDHA) was the dominant reaction. Finally, CPCs were fully converted to apatite except the cement with NaH_2PO_4 as liquid phase, because acidic environment inhibited the conversion of apatite. The pH increased linearly after mixing, when supersaturation was reached, it decreased to pH ≈ 6.0 gradually. Ultrasound measurement indicated that the variation of speed of sound (SOS) was related to both apatite formation and microstructural evolution. Ultrasonic attenuation coefficient (UAC) was able to quantitatively describe the curing process from viscous paste to elastic solid as a function of curing time. Moreover, the curing reaction conformed to classical dissolution-precipitation mechanism.

Y. Song · Z. Feng (✉) · T. Wang
Department of Materials Science and Engineering,
Xiamen University, Xiamen 361005, China
e-mail: zdfeng@xmu.edu.cn

1 Introduction

Calcium phosphate bone cement (CPC) as reported by Brown and Chow has attracted general attention [1], because CPCs show several advantages with respect to other materials that are used for bone repairs. For instance, they are injectable, and shaped easily. Therefore, they are very effective to fill bone defects with irregular shapes [2]. Moreover, CPCs are considered to be biocompatible and osteoconductive, so the new bone can grow into them when they are used as filling materials for bone defects [3]. Recently, various commercial CPCs have been introduced into the market [4, 5], and now they are frequently used in osseous reconstruction.

To reduce the risk of operation, and use CPCs more effectively, it is important to study the physicochemical properties variation during the curing of CPC. Additionally, it's critical to obtain high performance CPC, because the curing rate, degree and final product will influence the property of CPC. Several approaches have been developed to describe the curing of CPC, e.g., Gillmore needle for setting time [6], mechanical testing for compressive strength [7], and powder X-ray diffraction for phase conversion [8]. However, most of them cannot follow the curing process in real time, some of them are even destructive. As a result, the nature of these techniques fails to use to study the reaction of CPCs in situ. Therefore, real time monitoring techniques are required to track the curing process. Sarda et al. applied creep testing performed at low shear stress to study the rheological behavior of CPC paste during their initial stage, influence of some factors on the process was also explored [9]. However,

they didn't track the later stage of curing reaction. Quantitative ultrasonic measurement (QUS) that was once carried out for bone assessment and ordinary cement investigation now is also applied to study the curing process of bone cement [10–12]. Viano et al. investigated PMMA bone cements containing different hydroxyapatite concentration. Setting time was determined by the speed of the sound (SOS) and broadband ultrasonic attenuation (BUA). The results agreed well with the setting time obtained by conventional method [13]. In other papers [14, 15], more ultrasonic parameters such as adiabatic bulk modulus, acoustic impedance and density were studied in two different cements, pure α-calcium sulfate hemihydrate (CSH) and a mixture of α-tricalcium phosphate (α-TCP) and CSH. However, SOS couldn't be obtained in the cement based on α-TCP owing to the high attenuation, and the attenuation of cements was not studied as well [14, 15]. In situ XRD measurement was demonstrated to be an effective method for kinetic studies [16, 17], but there is no paper relating the investigation of the curing process of CPC using the method with an internal standard.

The present paper reports an in situ study of the curing of CPC in a simulative environment. Acoustic waves were transmitted into CPCs to follow the curing process, phase evolution and pH variation were also investigated throughout the whole process. By this method, it was able to describe the continuous curing process of CPC.

2 Materials and methods

2.1 Calcium phosphate bone cement

The CPC powder consisted of α-TCP, dicalcium phosphate dehydrate (DCPD) and calcium carbonate (CC). α-TCP was synthesized by the method reported in the relevant article [18], phase purity was confirmed by powder X-ray diffraction (PDF: 29–0359). Low crystallinity HAP was also added in CPC powders as a crystal seed, which was prepared by aqueous precipitation method in a basic environment [19]. Before the mixing of cement, all the reactants were milled separately in an agate ball mill to ensure rapid chemical reaction during the cement curing. The weight proportion and particle size of the four types of CPC powders used in this study are summarized in Table 1. About 2.5 wt% Na_2HPO_4 was dissolved in distilled water as one liquid phase (0.178 mol/l), another liquid phase was the aqueous solution of 0.178 mol/l NaH_2PO_4, the pH of them was 9.07 and 4.42, respectively [20–22]. Cements were prepared by mixing CPC powders and liquid phase at a liquid to power ratio of 0.39 ml/g. The cement mixed with two aqueous solutions was coded as cement-Na_2HPO_4 and cement-NaH_2PO_4 respectively in context.

2.2 Setting time

The final setting time (t_F) was determined by Gillmore needle method [23]. And cohesion time (t_C) was defined as the minimum time for CPC to obtain the ability to anti-washout [24].

2.3 Compressive strength

The cement pastes were mixed for 1 min, and then poured into molds (ϕ8mm × 23mm). After the lapse of cohesion time (t_C), the samples were demoulded and immersed in physiological saline at 37 °C. After soaked for fixed time intervals, the compressive strength of the cured samples was measured at a loading rate of 0.5 mm/min by using a mechanical testing system after the cylinders were polished on both sides. The fragments were put into 100% ethanol immediately, and freeze-dried for SEM observation.

2.4 In situ X-ray diffraction analysis

After being mixed for 1 min, the CPC paste containing high crystallinity SiO_2 was poured into the rectangle groove (5 × 10 mm in size and 1 mm in depth) of an aluminum slice. Data was collected [PANalytical X'Pert pro; 40 kV; 30 mA; integration time: 10 s; step scanning: 0.016° (2θ); $10° \le 2\theta \le 50°$] at the selected intervals. To ensure continuous curing reaction, the

Table 1 The weight proportion and particle size of cement powders

	α-TCP	DCPD	CC	HAP
Weight Proportion (wt%)	76.65	16.21	4.14	3.00
Particle Size [d0.5 (d0.1, d0.90)][a] (um)	2.94(1.86, 4.05)	23.87(3.84, 75.77)	2.01(0.47, 5.39)	<0.05 um

[a] The median particle size, d (0.5)—the particle size for which 50% of the sample volume was formed by particles that were smaller. The d (0.1) and d (0.9) were the particle size for which 10 and 90% of the sample volume were formed by particles that were smaller, respectively

data should be collected as soon as possible, and after each measurement, the CPC samples should be immediately put back into given curing environment prior to subsequent measurement. To prevent washout, all samples were stored in a 37 °C, 100% humidity container for the first 1 h, and then put in physiological saline at 37 °C. The degree of reaction and extent of conversion in curing process were estimated by quantitative X-ray diffraction analysis with SiO_2 as internal standard. The peak area of related peaks of SiO_2 at 26.64° (101), α-TCP at 30.71° (034), DCPD at 11.68° (020), CC at 29.41° (104), CDHA at 31.72° (211) without overlap were calculated to determine the relative content of these phases through I_{phase}/I_{SiO2}.

2.5 pH measurement

The pastes were prepared from 1.5 g CPC powders with liquid phase at L/P of 0.39 ml/g. After the lapse of cohesion time (t_C), the cement samples were removed from molds, and then immersed in 25 ml physiological saline at 37 °C. While stirring, a digital pH meter was applied to follow the pH variation and the pH was recorded after it reached equilibration. However, the samples weren't disintegrated in the whole curing process.

2.6 Ultrasonic measurement

Figure 1a shows an ultrasonic wave propagation model for the pulse-echo technique. Two transducers (Panametrics, v306, 2.25 MHz/0.5 inch in diameter) were connected to an ultrasonic pulser-receiver (Panametrics 5800) operated in a through-transmission mode. Signals were captured using a digital storage oscilloscope (Tektronix TDS 220), and then transferred to a personal computer. LabVIEW was used to develop the software for data acquisition and analysis. All samples were measured under the same experimental conditions, i.e., pulse repetition frequency (PRF) was set to 80 Hz and excitation energy 50 μJ.

To calibrate the setup of the system, aluminum alloy, stainless steel and brass standard blocks with different thickness were tested before the monitoring experiments. Because the diameters of samples were smaller than transducers', a foam barrier was applied to block off the ultrasound beam to avoid detection of unattenuated ultrasonic signals (Fig. 1b). Ultrasound started to monitor the curing process of CPC when the samples were demoulded after cohesion time (t_C), and the measurements were operated in degassed water at 37 °C. More than five CPC samples of each group were used for testing the final setting time (t_{F_SOS}), which was defined as the time when the first flex appeared in SOS curve.

2.7 SEM observation

To investigate the microstructural evolution of CPC, SEM (LEO-1530) was used to observe the surface morphology of freeze-dried samples after compressive strength measurement. Prior to observation, the fractured faces of CPC were sputter-coated with gold.

3 Results and discussion

Unlike ex situ measurement, in situ technique allows the analysis of a same sample from the beginning to the end of reaction, and avoids the influence of the different curing rate among samples. Moreover, less treatment is performed on samples before measurement, and the testing is carried out in the reaction environment. It is able to follow the curing process continuously and obtain information on time.

3.1 Final setting time and compressive strength

Table 2 shows the curing properties of two cements. Each group consisted of at least three parallel effective samples. Statistical analysis indicated that both groups were significantly different for all the properties ($p < 0.05$). Moreover, cement-Na_2HPO_4 had higher

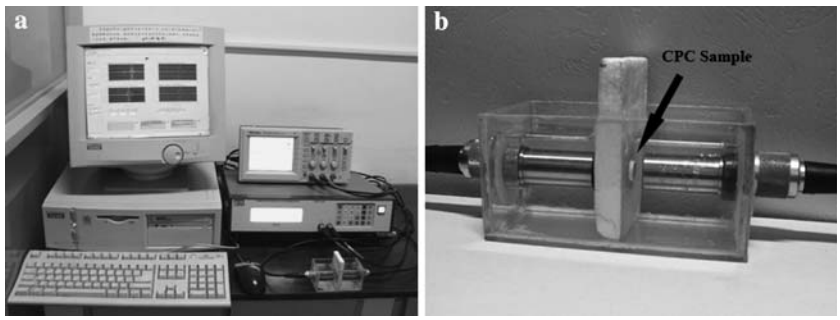

Fig. 1 The structure of ultrasonic pulse-echo measurement system for in situ investigation, foam in the water cell was used to prevent the unattenuated signals

Table 2 Comparison of curing properties for two cements

Liquid Phase	t_C (min)	t_F (min)	t_{F_SOS} (min)	CS (MPa)
Na_2HPO_4	7.2 ± 0.8	10.8 ± 1.3	16.1 ± 0.4	45.3 ± 1.6
NaH_2PO_4	8.8 ± 0.8	14.8 ± 1.6	17.5 ± 0.3	36.1 ± 2.1

performance, and satisfied clinical requirement [24]. It also indicated that the t_{F_SOS} of two cements were slightly higher than the values (t_F) obtained by the conventional Gillmore needle method, and there was significant difference between t_F and t_{F_SOS} ($p < 0.05$), the reason might be errors between instruments and the different curing condition.

3.2 Kinetics analysis

The phase evolution of CPCs is displayed in Fig. 2, where the time intervals represent curing durations of the same sample at 37 °C. At the beginning of reaction, several sharp and high diffraction peaks corresponding to initial CPC powders were presented in the XRD spectra. Afterwards, the peaks decreased and broadened, and a small amount of CHA was found in the cement after 2 h. However, the main peak of CHA at $2\theta = 32.17°$ (112) overlapped with that of α-TCP corresponded to the 4 reflection, so the value of peak area could not be exactly calculated. The formation of CDHA in CPC was evidenced by the presence of a peak at $2\theta = 31.72°$ (211) in XRD patterns. Although CDHA was detected after cement curing for a longer while, the intensity of the CDHA peaks increased much faster and finally exceeded that of CHA. The whole reaction was completed in three days (72 h), CHA and CDHA with small crystallite size were the main phases in the products.

In order to study the reactive rate quantitatively, the variation of the relative content of α-TCP, DCPD and CC, as well as the hydrated phases CDHA are summarized in Fig. 3–4. Some deviated points might result from the influence of water content and the difference of testing area. Curve fittings were made for all of data points in figures.

CC phase was firstly exhausted in cements (Fig. 3a). About half of CC reacted in the first 2 h, and the remainder disappeared in the next 6 h. Compared with cement-Na_2HPO_4, CC reacted more rapidly in cement-NaH_2PO_4 especially in the early stage. It may be ascribed to the acidic liquid phase of cement-NaH_2PO_4. Figure 3b displays the reactive process of DCPD. Similarly, a significant amount of DCPD reacted in the first 6 h, and the DCPD phase could not be detected any more in the cement after 24 h, which is quite different from DCP-α-TCP system in which DCP is an unreactive phase in the mixture [18]. Therefore, α-TCP

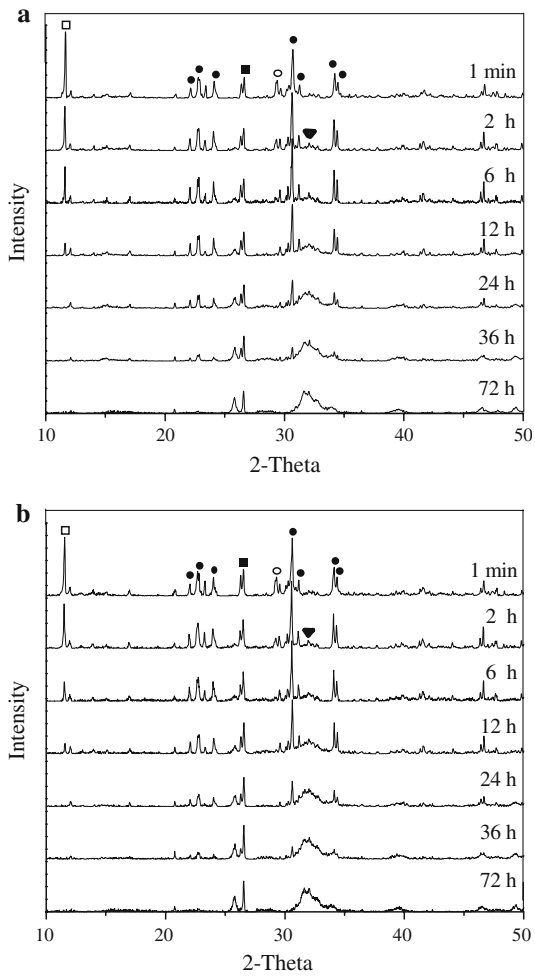

Fig. 2 Evolution of X-ray diffraction patterns for two calcium phosphate cements (CPCs) incubated at 37 °C, a. cement-Na_2HPO_4 b. cement-NaH_2PO_4 (□, DCPD; ●, α-TCP; ○, CC; ■, SiO_2; ▼, CHA; * CDHA)

was the only substrate in original CPC powder that existed throughout the 72 h reaction, and the curing speed was controlled by α-TCP. Based on solubility phase diagrams of calcium phosphates [25], DCPD and α-TCP has a higher solubility in low pH when pH < 8.0, so the two powders dissolved faster in cement-NaH_2PO_4 (Fig. 3b and c).

The previous discussion has indicated that CHA was the dominant new phase in early stage, but the subsequent formation of CDHA displayed higher rate of conversion and exceeded CHA in intensity. The phenomenon may be attributed to the absence of CC that was the source of supply of CO_3^{2-}. When most of

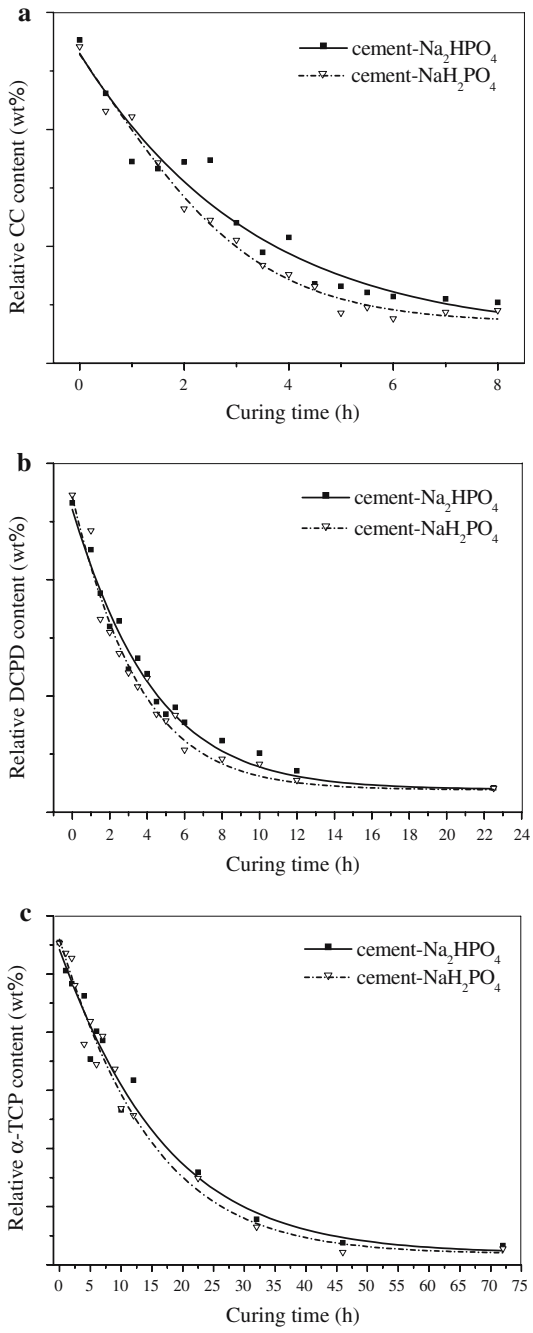

Fig. 3 Relative amount of CPC components as a function of curing time (**a**) calcium carbonate (CC) (**b**) dicalcium phosphate dehydrate (DCPD) (**c**) α-tricalcium phosphate (α-TCP)

the CC had been consumed, CHA would not form in the region lacking CO_3^{2-}, other types of apatite such as CDHA would present instead. On the other side, the content of CHA still increased after exhausting of CC. The phenomenon may be attributed to the fact that a portion of CC converted to some amorphous substances, because none of new phases containing CO_3^{2-} was detected in XRD spectra. However, evidence of the assumption need to be explored in further study. And the other reason for CHA increase might be the CO_2 of atmosphere dissolved into the aqueous solution [26]. Figure 4 displays the conversion of CDHA as a function of time. In the early stage, the amount of CDHA was negligible. The time required for the formation of detectable CDHA was longer for cement-NaH_2PO_4, which may be related to its lower pH value. And then the amount of CDHA increased linearly with time until a flat plateau was reached. However, there was more CDHA in cement-Na_2HPO_4 than cement-NaH_2PO_4 in the final products. A small amount of octocalcium phosphate (OCP) was also detected in the final products of cement-NaH_2PO_4. Acidity environment is unfavorable for apatite conversion.

Figure 5 reveals the pH variation versus the curing time for the two cements. The initial increase in pH was probably due to the dissolution of three basic CPC powders, namely α-TCP, DCPD and CC. However, under the influence of acidic aqueous solution of

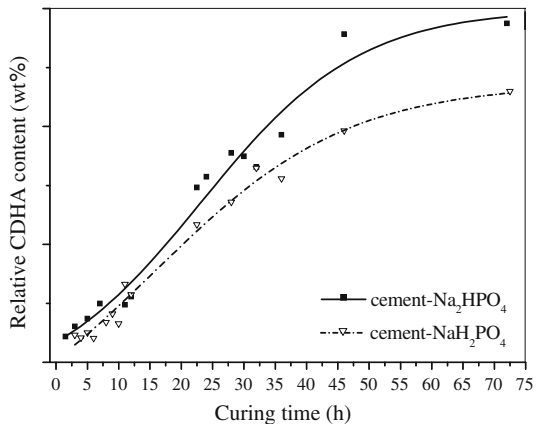

Fig. 4 Relative amount of calcium deficient hydroxyapatite (CDHA) in two cements as a function of curing time

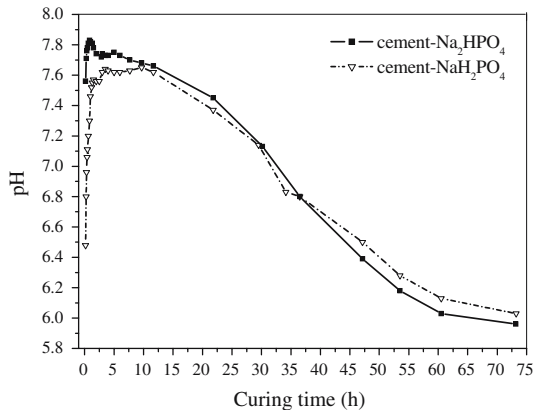

Fig. 5 pH variation with time of curing in physiological saline at 37 °C

cement-NaH_2PO_4, the beginning pH value for cement-NaH_2PO_4 was only 6.48, which was much lower than that for cement-Na_2HPO_4 (pH = 7.58). And for the same reason, pH increased more rapidly in cement-NaH_2PO_4, a similar conclusion was also obtained in XRD analysis. It is well known that the solubility of the reactants and the supersaturation of the solution control the precipitation of the reaction product. Although CPC powders in cement-NaH_2PO_4 had higher dissolution rate, the starting pH was lower. As a result, more time was required for cement-NaH_2PO_4 to reach certain supersaturation degree and for apatite to start forming. Afterwards, pH continuously decreased upon the hydration of α-TCP and the formation of apatite [27]. But the pH kept on descending beyond 7.0, it was mainly determined by the partial dissolution of apatite. The dissolution of CO_2 from atmosphere attributed to the decrease of pH value as well. Equilibrium was finally reached between apatite formation and dissolution, and the final pH was close to 6.0.

3.3 Ultrasonic measurement

The mixture of different granule size made the ultrasonic attenuation of the studied CPC system much less than that of the pure α-TCP system. Therefore, it was possible to obtain accurate ultrasonic waveshapes from very beginning to several days.

Figure 6 shows the variation of SOS for two cements. The SOS plots reveal three significant phases in the whole curing process. A steep rise was shown at the beginning of measurement, then the increasing rate decreased with the development of curing reaction, finally, SOSs came into a flat period after slight descending. The first two stages were similar to corresponding data reported in literatures [13–15]. However, the last stage of SOS variation has not been reported. To the best knowledge of the authors, no experiment has been successfully conducted to track the whole curing reaction of CPC by QUS so far.

Similar to the traditional Portland cement [28, 29], CPCs had a good exponential relationship between SOS and CS during the curing process (Fig. 7). Therefore, the SOS variation could be applied to approximately estimate the change of mechanical strength of CPC. At the beginning of measurement, the SOS of cement-Na_2HPO_4 was 59.68 m/s higher than that of cement-NaH_2PO_4, it meant that the cement-Na_2HPO_4 was stiffer than cement-NaH_2PO_4. The fact could also be supported by the final setting time of two cements deduced from SOS plots, i.e., 16.1 ± 0.42 min for cement-Na_2HPO_4 and 17.5 ± 0.35 min for cement-NaH_2PO_4. The final setting time was the time when cements had enough stiffness to resist the fixed pressure. Therefore, cement-Na_2HPO_4 would obtain much higher mechanical strength in the same curing time as compared with cement-NaH_2PO_4. And cement-Na_2HPO_4 maintained the higher stiffness in the whole process because the SOS of which was always higher than that of cement-NaH_2PO_4. Actually, both the variation of SOS and CS were influenced by change of microstructure in CPC. From the results of XRD analysis in the early stage, little apatite was presented in CPC. However, Fig. 8a and b indicate that CPC powders dissolved and connected with each other during the first 40 min. Compared with Fig. 8a, the pores in Fig. 8b were less and smaller, because CPC powders dissolved and filled in the spaces among them. As this process continued, the air bubbles and liquid phase in the pores would also diminish. The air bubbles were formed in the period of CPC preparation. All of these factors would cause the rapid increasing of SOS

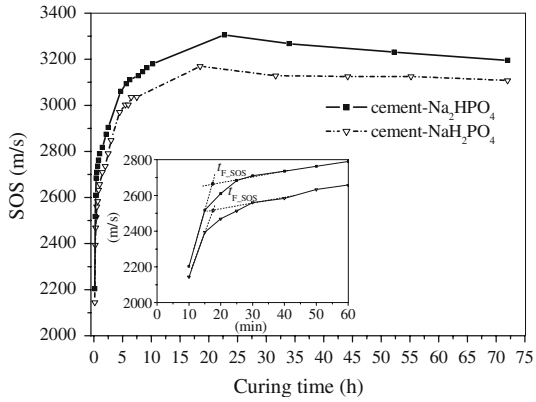

Fig. 6 Variation in speed of sound (SOS) as a function of curing time

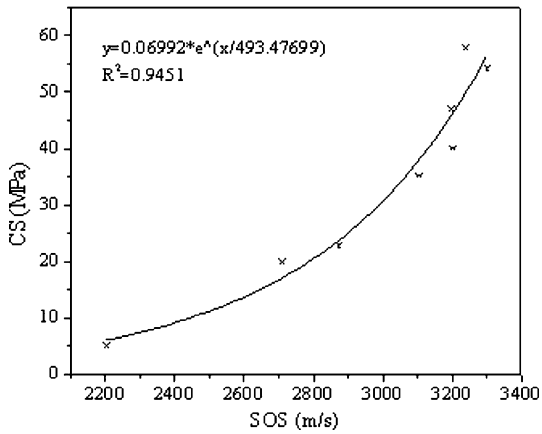

Fig. 7 Relationship between compressive strength (CS) and speed of sound (SOS)

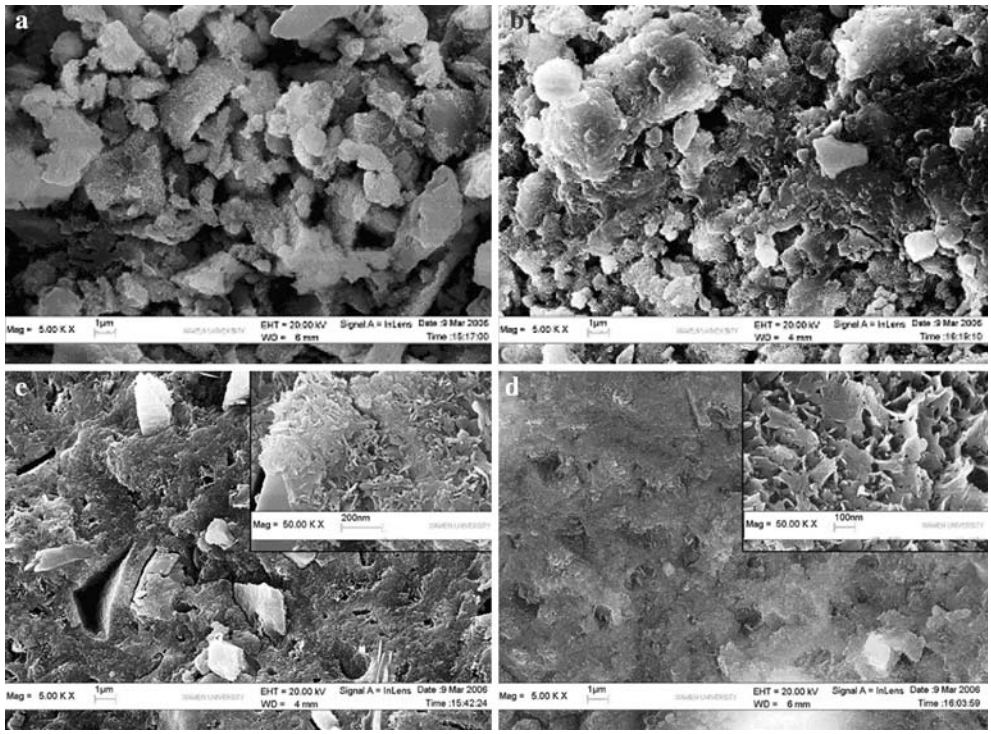

Fig. 8 Scanning electron microscope (SEM) micrograph of the fracture surface for (a) 10 min, (b) 40 min, (c) 24 h and (d) 72 h

in the first stage [30]. At the second stage, the SOS increased at a decreasing rate. The phenomenon mainly resulted from the formation of apatite crystals, which increased the physical contact points among unreacted particles and thereby improved mechanical strength (Fig. 8c). As soon as the grains are linked together, the skeleton becomes more rigid, which induces an increase in the velocity of US. However, the rate of precipitation was slower compared with that of the dissolution in the first stage. Figure 8c displays the fracture surface of the cement cured for 24 h. XRD and SEM analysis indicated that the remainder particles on the fracture surface might be the unreacted α-TCP powders. The slight decrease of SOS at the third stage related to the change of the CS during the curing of CPC [31]. Although the amount of apatite phases increased in the initial hours of the third stage, the microstructure evolution in this stage was harmful to mechanical strength and led to the descending of SOS. According to dissolution-precipitation model suggested by Shen et al. [32], the unreacted powders would be enwrapped by apatite crystals in the precipitation process. When water penetrated through the apatite layers and reacted with powders inside, the previous interconnected porous structure would be destroyed. Figure 8d indicates that all these particles disappeared after cement cured for 72 h, and some micropores were presented in CPC. As observed by SEM under 50000×, a platelike morphology of apatite could be observed in CPC.

Figure 9 displays the attenuation plot of CPC as the function of curing time. Unlike the attenuation curve of PMMA bone cement reported by Viano et al. [13], no attenuation peak was presented in the UAC plot of CPC. In this case, UAC was characterized by a sharp initial decrease, followed by a relatively slow decrease until a plateau value.

US attenuate when it transits through samples, converting portion of mechanical energy into heat

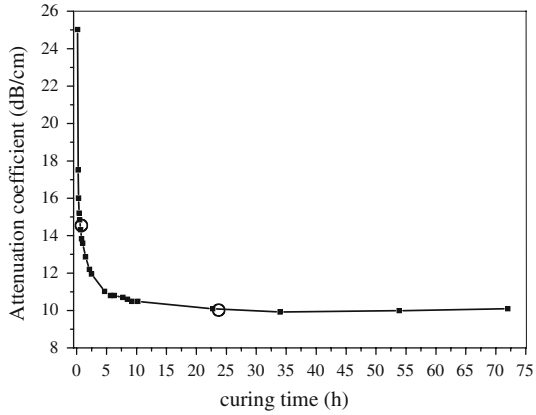

Fig. 9 Variation in ultrasonic attenuation coefficient (UAC) as a function of curing time

energy. Some factors, such as the granule, granule reaction, the evolution of the size and distribution of pores affect the dissipation of energy, but the main reason of attenuation during the curing reaction may be the internal friction and the presence of air bubbles [33]. Just after mixed, the cement showed viscous behavior. At this stage most of CPC powders did not dissolve so they were separated and had the largest area of the interface between granules (Fig. 8a). When compressional waves transited through CPC, the friction between granules exhausted most of the energy, and the presence of air bubbles in pores also caused a strong attenuation of mechanical waves. As a result, the amplitude of US was extremely low, sometimes even no ultrasonic signals could be detected. Afterwards, most of CPC powders started to dissolve and the remainders connected together. In this process, some macropores in CPC would gradually filled by the paste and others were replaced by several micropores (Fig. 8b). With the increasing degree of connectivity, a gel structure was presented in CPC and the interface slippage reduced. The kinetic analysis stated above indicated that the CPC powders dissolved rapidly at the very early stage, so a steep decrease was displayed at the beginning of UAC plot. When the solution reached supersaturation, apatite phases began to precipitate. With the increasing of interconnection among unreacted particles, a precipitation matrix would form in CPC (Fig. 8c). Because less and less powders were reserved with the gradual dissolution reaction, the action of friction diminished, and it resulted in UAC decreasing at a lower rate. After CPC became an elastic solid, most of powders dissolved and the surface area was no more the main influence factor for energy dissipation. The succeeding dissolution-precipitation process also had little influence on the variation of UAC. However, wave propagation in such systems is quite complicated. Different mechanisms contribute to the total attenuation. Further study is required in this aspect.

4 Conclusions

In this paper, several techniques were employed to follow the entire curing process of CPC in a simulative environment. The variation of physicochemical properties of CPC during the curing was studied systematically, and the influence of liquid phase on the curing properties was explored as well.

The curing process of CPC can be described as follows: (a) At the early stage, although CPC powders dissolved rapidly and pH increased sharply, little apatite phases were formed in CPC. However, due to the dissolution of granules, the CS increased and the UAC decreased. (b) After supersaturation was reached in the solution, apatite phases started to form in neutral condition and pH began to descend. In addition, the UAC decreased at a lower rate with the precipitating of apatite phase. The mechanical strength in this stage mainly resulted from apatite formation. (c) At the last stage, although the amount of apatite increased continuously, the dominant change was the formation of porous structure in CPC, which led to the slight decrease of mechanical strength. The UAC was almost constant in this stage.

Liquid phase is one of the most effective methods to alter the reactive environment for CPC powders. Kinetic study showed that liquid phase affected both the reactive rate and the final products. Cement with Na_2HPO_4 as liquid phase favored the conversion of apatite, and resulted in higher compressive strength. The results will be helpful for both CPC modification and application.

Acknowledgments This work is financially supported by the National Natural Science Foundation of China (30470434).

References

1. W. E. BROWN and L. C. CHOW, *US Pat.* 4518430 (1985)
2. M. BOHNERA and G. BAROUD, *Biomaterials* **26** (2005) 1553
3. B. R. CONSTANTZ, I. C. ISON, F. M. FULMER, R. D. POSER, S. T. SMITH, T. SUSANNE, M. VANWAGONER, R. JOHN, S. A. GOLDSTEIN, J. B. JUPITER and D. I. ROSENTHAL, *Science* **267** (1995) 1796
4. M. BOHNER, *Eur Spine J.* **10** (2001) S114
5. M. BOHNER, *Injury, Int. J. Care Injured* **31** (2000) S-D37
6. E. FERNANDEZ, F. J. GIL, M. P. GINEBRA, F. C. M. DRIESSENS, J. A. PLANELL and S. M. BEST, *J. Mater. Sci. Mater. Med.* **10** (1999) 223
7. E. FERNANDEZ, F. J. GIL, S. M. BEST, M. P. GINEBRA, F. C. M. DRIESSENS and J. A. PLANELL, *J. Biomed. Mater. Res.* **41** (1998) 560
8. E. FERNANDEZ, M. P. GINEBRA, M. G. BOLTONG, F. C. M. DRIESSENS, J. GINEBRA, E. A. P. DE MAEYER, R. M. H. VERBEECK and J. A. PLANELL, *J. Biomed. Mater. Res.* **32** (1996) 367
9. S. SARDA, E. FERNANDEZ, J. LLORENS, S. MARTINEZ, M. NILSSON and J. A. PLANELL, *J. Mater. Sci. Mater. Med.* **12** (2001) 905
10. S. HAN, J. MEDIGE, K. FARAN, Z. FENG and I. ZIV, *Med. Eng. Phys.* **19** (1997) 742
11. D. HANS, C. WU, C. F. NJEH, S. ZHAO, P. AUGAT, D. NEWITT, T. LINK, Y. LU, S. MAJUMDAR and H. K. GENANT, *Calcif. Tissue. Int.* **64** (1999) 18
12. J. R. RAPOPORT, J. S. POPOVICS, S. V. KOLLURU and S. P. SHAH, *ACI. Mater. J.* **97** (2000) 675
13. A. M. VIANO, J. A. AUWARTER, J. Y. RHO and B. K. HOFFMEISTER, *J. Biomed. Mater. Res* **56** (2001) 593

14. M. NILSSON, J. CARLSON, E. FERNANDEZ and J. A. PLANELL, *J. Mater. Sci. Mater. Med.* **13** (2002) 1135
15. J. CARLSON, M. NILSSON, E. FERNANDEZ and J. A. PlANELL, *Biomaterials* **24** (2003) 71
16. J. WIENOLD, R. E. JENTOFT and T. RESSLER, *J. Synchrotron Radiat.* **8** (2001) 677
17. O. KIRILENKO, F. GIRGSDIES, R. E. JENTOFT and T. RESSLER, *Eur. J. Inorg. Chem.* **11** (2005) 2124–2133
18. I. KHAIROUN, F. C. M. DRIESSENS, M. G. BOLTONG, J. A. PLANELL and R. WENZ, *Biomater.* **20** (1999) 393
19. A. C. TAS, F. KORKUSUZ, M. TIMUCIN and N. AKKAS, *J. Mater. Sci. Mater. Med.* **8** (1997) 91
20. E. FERNANDEZ, M. NILSSON, S. SARDA, L. LIDGREN and J. A. PLANELL, *J. Biomed. Mater. Res.* **61** (2002) 600
21. M. TAKECHI, Y. MIYAMOTO, K. ISHIKAWA, M. NAGAYAMA, M. KON, K. ASAOKA and K. SUZUKI, *J. Biomed. Mater. Res.* **39** (1998) 308
22. K. ISHIKAWA, S. TAKAGI, L. C. CHOW and K. SUZUKI, *J Biomed Mater Res.* **46** (1999) 504
23. Standard test method for time of setting of hydraulic cement paste by the Gillmore needles, ASTM C266–89, Annual Book of ASTM Standards, Vol. 04.01: Cement, Lime, Gypsum. Philadelphia: ASTM (1993) 189
24. E. FERNANDEZ, M. G. BOLTONG, M. P. GINEBRA, F. C. M. DRIESSENS, O. BERMUDEZ and J. A. PLANELL, *J. Mater. Sci. Lett.* **15** (1996) 1004
25. E. FERNANDEZ, F. J. GIL, M. P. GINEBRA, F. C. M. DRIESSENS, J. A. PLANELL and S. M. BEST, *J. Mater. Sci. Mater. Med.* **10** (1999) 169
26. E. FERNANDEZ, J. A. PLANELL, S. M. BEST and W. BONFIELD, *J. Mater. Sci. Mater. Med.* **9** (1998) 789
27. E. FERNANDEZ, F. J. GIL, M. P. GINEBRA, F. C. M. DRIESSENS, J. A. PLANELL and S. M. BEST, *J. Mater. Sci. Mater. Med.* **10** (1999) 223
28. R. DEMIRBOGA, I. TURKMEN and M. B. KARAKOC, *Cem. Concr. Res.* **34** (2004) 2329
29. L. M. DEL RIO, A. JIMENEZ, F. LOPEZ, F. J. ROSA, M. M. RUFO and J. M. PANIAGUA, *Ultrasonics.* **42** (2004) 527
30. T. CHOTARD, N. GIMET-BREART, A. SMITH, D. FARGEOT, J. P. BONNET and C. GAULT, *Cem. Concr. Res.* **31** (2001) 405
31. C. S. LIU, W. SHEN, Y. F. GU and L. M. HU, *J. Biomed. Mater. Res.* **35** (1997) 75
32. W. SHEN, C. S. LIU and Y. F. GU, *Daqing Shiyou Xueyuan Xuebao.* **22** (1998) 129
33. A. BOUMIZ, C. VERNET and F. COHEN TENOUDJI, *Adv. Cem. Based. Mat.* **3** (1996) 94